CrystEngComm

Accepted Manuscript

Journal Name

ARTICLE

3D AgCl Microstructures Selectively Fabricated via a Cl⁻-Induced Precipitation from [Ag(NH₃)₂]⁺

Harnchana Gatemala, Chuchaat Thammacharoen, Sanong Ekgasit[*]

Herein various AgCl microstructures including octapods, octapods with fishbone pods, hexapods, hexapods with 4-blade arrowhead pods, concave octahedrons, and octahedrons are selectively precipitated from $[Ag(NH_3)_2]^+$ solution by an addition of Cl⁻. The microstructures were rapidly formed and precipitated within 5 min. In a Cl⁻-rich environment, the octapod grew from cubic seeds as the growth along <111> directions was favorable. The hexapod grew from octahedral seeds in an NH_4OH-rich environment as the growth along <100> directions was dominated. By manipulating the seed morphology and the growth environment, complex AgCl microstructures of thermodynamically unfavorable structures (hexapods and octahedrons) can be selectively fabricated. A potential application as a photocatalyst of AgCl microstructures was explored by a partial photo-reduction of the surface AgCl into isolated AgNPs. The fabricated AgCl microstructures were turned into an efficient Ag@AgCl visible-light photocatalyst as a completed decomposition of methyl orange was achieved within 20 min. This work not only explores a method to control the preferential growth along <100> and <111> directions of AgCl microstructures, but also provides an in-depth understanding on the crystal growth mechanisms and how to manipulate them efficiently.

Introduction

Morphology-controlled synthesis of inorganic materials has attracted significant research attention as their physical, chemical, optical, magnetic and catalytic properties can be tuned by tailoring their size, shape, and composition.[1] Highly-branched inorganic micro/nanostructures synthesized by induced anisotropic growth[2] and selective etching method[3, 4] have been studied. For example, octapod Pt nanocrystals fabricated via an environmentally controlled wet chemical synthesis exhibited particularly high activity in formic acid oxidation.[2, 5, 6] Morphology-controlled synthesis has focused on the fabrication of structures with high-index facets in order to enhance the photocatalytic activities. Pd and Pt crystals, having crystal growth along <111> and <100> directions, showed exceptionally high electrocatalytic activities due to high index facets including {720}, {730}, {520}, and {830}.[7-9]

Silver chloride (AgCl) is well-known as a photosensitive material in photographic industry and imaging. A recent discovery of its excellent visible light photocatalytic activity derived from the surface plasmon resonance (SPR) induced electron transfer triggered by the surface silver nanoparticles has drawn considerable further researches.[10-16] Various AgCl micro/nanostructures including nanoparticles,[17] nanospheres,[18] nanocubes,[10, 18-21] and caged cubes[22] were synthesized and explored for potential applications as advanced functional material. A morphology-controlled synthesis of concave cubic and 3D AgCl hierarchical superstructure via the facet selective growth protocol has been demonstrated.[23, 24] To allow a slow crystal growth, the oxidation-controlled release of Ag⁺ in a solution with high Cl⁻ concentration was performed. The kinetic growth along the <111> and <100> directions of the cubic seeds enables a formation of concave cubes and AgCl hierarchical superstructures as the surface energies of the Cl⁻-bonded {100} facets are much greater than those of the Cl⁻-bonded {110} and {111} facets. Interestingly, the 3D AgCl hierarchical superstructures show a better photocatalytic activity compared to those of cubes and concave cubes. To explore and realize the potential applications offered by the novel structural controlled materials, efficient methods for the fabrication of precisely controlled complex micro/nanostructures are still required.

In this contribution, we present a strategic morphology-controlled synthesis that enables a selective fabrication of 3D AgCl microstructures from silver ammine ($[Ag(NH_3)_2]^+$) complex by an addition of Cl⁻. The 3D AgCl microstructures including octapods (8pAgCl), 8pAgCl with fishbone pods, hexapods (6pAgCl), 6pAgCl with 4-blade arrowhead pods, concave octahedrons, and octahedrons could be selectively precipitated and separated. The photocatalytic activity of the synthesized 3D AgCl microstructures were explored by a decomposition of methyl orange (MO) solution under a visible-light irradiation.

Experimental Section

Chemicals: Silver nitrate (AgNO₃≥99.8%), sodium chloride (NaCl≥99%), ammonium hydroxide solution (NH₄OH 25% w/w) and methyl orange (MO) were purchased from Merck® and were used as received. Prior to use, all glassware and

magnetic bars were thoroughly cleaned with detergent, rinsed with deionized (DI) water, rinsed with 6 M nitric acid, and thoroughly rinsed with DI water.

Synthesis of 3D AgCl microstructures: Various 3D AgCl microstructures were selectively synthesized via a Cl⁻-induced precipitation from silver ammine ($[Ag(NH_3)_2]^+$) complex precursor. Briefly, a solution of $[Ag(NH_3)_2]^+$ was prepared by rapidly mixing AgNO₃ solution (0.1 M, 5 mL) with NH₄OH solution (5.308 M, 2.83 mL) under a vigorous stir. A dark brown colloid of silver (I) oxide (Ag₂O) was observed for a brief moment prior to the formation of a colorless solution of $[Ag(NH_3)_2]^+$ complex. To induce a formation of 3D AgCl microstructures, the complex solution was quickly poured into NaCl solution (1.08 M, 92.17 mL). The clear solution instantaneously turned milky white indicating a formation of solid AgCl. The colloid was then vigorously stirred for 5 min before allowing the solid AgCl to precipitate. The clear supernatant was decanted. The precipitate was 5-time washed with DI water and once with ethanol before drying under a dark ambient condition. Under this condition, the concentrations of AgNO₃, NaCl, and NH₄OH in the reacting medium were 5 mM, 1 M, and 0.15 M, respectively. To investigate the influence of Ag⁺, Cl⁻, and NH₄OH on the morphology of AgCl microstructures, their concentrations were systematically manipulated within the range of 2.5 - 10 mM, 0.1 - 2 M, and 0 - 0.3 M, respectively.

Selective etching of AgCl microstructures: The dissolution of certain crystallographic facet of AgCl microstructures under a continuous rinsing of NH₄OH solution (0.1 M for cubes and truncated cubes and 0.5 M for octahedrons) was performed. Briefly, precipitated AgCl was immobilized on filter paper by a simple filtration. The remaining AgCl on the paper was continuously rinsed by the NH₄OH solution. The structural changes were investigated after 1- and 2-min rinsing.

Structural transformation of AgCl microstructures: A colloid of cubic AgCl was prepared by mixing a solution of $[Ag(NH_3)_2]^+$ (i.e., prepared by mixing AgNO₃ (0.1 M, 5 mL) with NH₄OH (5.308 M, 1 mL)) with NaCl solution (6.5 mM, 100 mL). The AgCl cubes (average size of 1 - 2 μm) formed within 1 min. To induce a structural transformation, NH₄OH solution (5.308 M, 1 mL) was added into the colloid and the product was collected after 30 s, 1, 2, 5, 10, 30, and 120 min for further characterization.
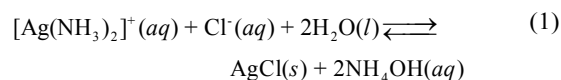
Characterization: Morphology (size and shape) of the 3D AgCl microstructures was recorded by a scanning electron microscope (SEM, JEOL JSM-6510A) operating at 20 kV under a high vacuum mode with a secondary ion (SEI) detector. The X-ray diffraction (XRD) patterns were collected by an X-ray diffractometer (Rigaku D/MAX-2200) operated at room temperature with a scanning rate of 0.02 deg/min, using Cu K_α irradiation (40 kV, 30 mA). The diffractograms were recorded within 20° - 80° region.

Photocatalytic activity investigation: A selected 3D AgCl microstructure (0.1 g) was mixed with methyl orange (MO) solution (20 mg/L, 100 mL). The mixture was incubated for 60 min in the dark. The photocatalytic activity under a visible light irradiation (250 W Xe arc lamp) was carried out. An aliquot (5 mL) was taken out every 2 min for visible adsorption measurement (USB4000 fiber optic spectrometer coupled with a DH-2000 deuterium/halogen light source, Ocean Optics).

Results and discussion

The $[Ag(NH_3)_2]^+$ solution prepared from AgNO₃ and NH₄OH is a colorless solution with excess NH₄OH. A precipitation of solid AgCl from the complex can be achieved by an addition of NaCl solution, as shown in Equation 1.[25]

$$[Ag(NH_3)_2]^+(aq) + Cl^-(aq) + 2H_2O(l) \rightleftharpoons$$

$$AgCl(s) + 2NH_4OH(aq) \quad (1)$$

The concentrations of NH₄OH, NaCl as well as AgNO₃ strongly affect the morphology (size and shape) of the precipitated AgCl. By systematically adjusting their concentrations, 3D AgCl microstructures including 8pAgCl, 8pAgCl with fishbone pods, 6pAgCl, 6pAgCl with 4-blade arrowhead pods, concave octahedrons, octahedrons, a mixture of small concave cubes, small 6pAgCl, and small 8pAgCl, and microspheres, as shown in Fig. 1, could be selectively precipitated.

According to the morphologies shown in Fig. 1 and S1, 3D AgCl microstructures with unique exposed surfaces could be selectively precipitated from $[Ag(NH_3)_2]^+$ complex under a controlled environment. Microstructures with symmetric pod length indicate a uniform crystal growth while the uniform sizes indicate a complete separation between the nucleation and growth periods in this one-pot synthetic protocol. Although AgCl is sparingly soluble in water ($K_{sp} = 1.77\text{x}10^{-10}$),[26] its
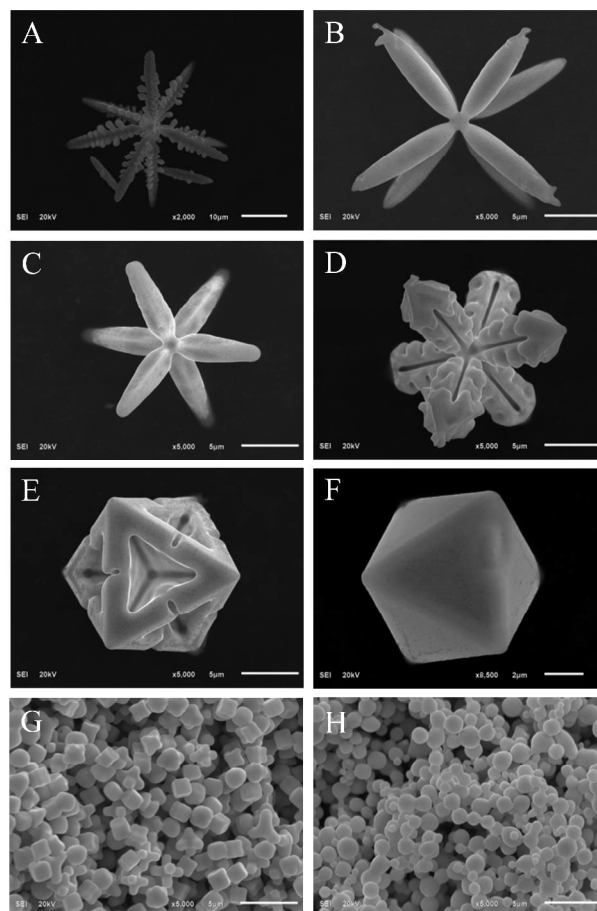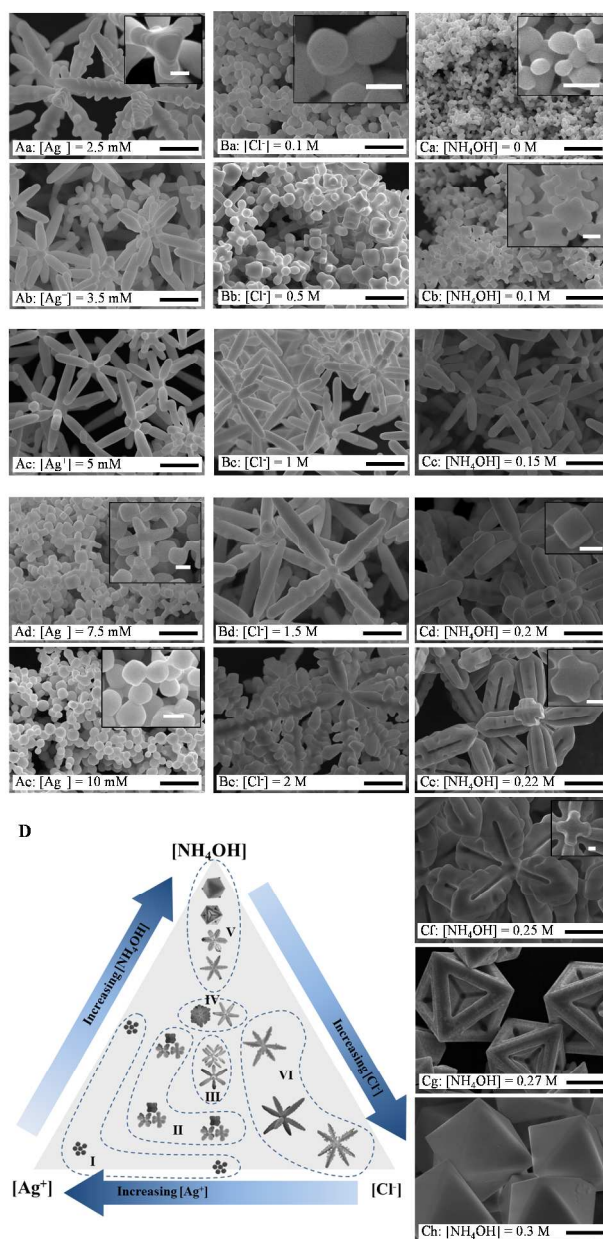

Fig. 1 AgCl microstructures precipitated from $[Ag(NH_3)_2]^+$ complex by an addition of Cl⁻: (A) 8pAgCl with fishbone pods, (B) 8pAgCl, (C) 6pAgCl, (D) 6pAgCl with 4-blade arrowhead pods, (E) concave octahedrons, (F) octahedrons (G) mixture of small concave cubes, small 6pAgCl, and small 8pAgCl, and (H) microspheres.

solubility in NH₄OH solution increases as it forms water soluble [Ag(NH₃)₂]⁺Cl⁻ complex.[27] As a result, a relatively high Cl⁻ concentration was necessary to induce the precipitation (Fig. S2). In an initial investigation, a clear solution of [Ag(NH₃)₂]⁺ complex was prepared by mixing AgNO₃ solution (0.1 M, 2.5 mL) with NH₄OH solution (5.308 M, 2.83 mL). The [Ag(NH₃)₂]⁺ complex solution was rapidly poured into NaCl solution (1.06 M, 94.67 mL) to induce a formation of solid AgCl. Under this condition the concentrations of Ag⁺, Cl⁻, and NH₄OH, respectively, were 2.5 mM, 1 M, and 0.15 M with the mole ratios [Cl⁻]/[Ag⁺], R1 = 400 and [NH₄OH]/[Ag⁺], R2 = 60. The precipitated 3D AgCl microstructure was 8pAgCl with fishbone triangular pods, as shown in Fig. 2Aa and Table 1. The precipitation of 8pAgCl was expected as the crystals were formed in an environment with high Cl⁻ concentration. The Cl⁻-rich environment promotes the growth in <111> directions of cubic seeds.[6, 23] As the concentration of Ag⁺ increased to 3.5 and 5 mM, a mixture of 8pAgCl and 6x4pAgCl were obtained (Fig. 2Ab and 2Ac). A mixture of small 8pAgCl, concave cubes, and 6pAgCl were obtained when Ag⁺ concentration increased to 7.5 mM (Fig. 2Ad). An instantaneous precipitation of AgCl microspheres occurred when Ag⁺ concentration increased to 10 mM (Fig. 2Ae).

The formation and growth of 8pAgCl with fishbone pods, 8pAgCl, and concave cubes from cubic seeds under the influence of Cl⁻ were clearly explained by Huang's group.[23, 24] In our investigation, the formation of eight-pod family from cubic seeds in Cl⁻-rich environment is expected. However, the co-precipitation of 6pAgCl and 6x4pAgCl in Fig. 2Ab - 2Ad was unexpected since they could not grow from the cubic seeds. The formation of six-pod family could be associated with the presence of NH₄OH.

In Fig. 2B, the influence of Cl⁻ concentration was verified over the range of 0.1 - 2 M corresponding to R1 = 20 - 400 (the concentrations of Ag⁺ and NH₄OH were fixed at 5 mM and 0.15 M, respectively). At low Cl⁻ concentration of 0.1 M (Fig. 2Ba) AgCl microspheres with an average diameter of 1 μm instantaneously precipitated. At Cl⁻ concentration of 0.5 M (Fig. 2Bb), the product was a mixture of 6pAgCl with an average pod length of 2 μm, concave cubes with an average size of 2.5 μm, and 8pAgCl with an average pod length of 1 μm. However, when the Cl⁻ concentration increased to 1.5 M (Fig. 2Bd), the large 8pAgCl with an average pod length of 10 μm was the sole product. At an extremely high Cl⁻ concentration of 2 M (Fig. 2Be), 8pAgCl with 10-μm long fishbone triangular pods was obtained. This morphology is in good agreement with that in Fig. 2Aa as they were precipitated at the same R1 (see Table 1).

The influence of NH₄OH concentration was conducted over 0 - 0.3 M while the concentration of Ag⁺ and Cl⁻ were fixed at 5 mM and 1 M (R1 = 200 and R2 = 0 - 60), respectively. In the absence of NH₄OH (Fig. 2Ca), AgCl microspheres with an average size of 500 nm instantaneously precipitated. At 0.1 M NH₄OH (Fig. 2Cb), a mixture of small 8pAgCl, small concave cubes, and small 6pAgCl was obtained. At 0.2 M NH₄OH (Fig. 2Cd), the precipitate consisted of 6pAgCl and 8x3pAgCl. At 0.22 and 0.25 M NH₄OH (Fig. 2Ce and 2Cf), the product was 6pAgCl with 4-blade arrowhead pods. The 4-blade pods originated from crystal growth in the <100> directions along the pod length. The grove between adjacent blades on the same pod was the growth-suppressed {110} facets. As NH₄OH concentration increased to 0.27 M (Fig. 2Cg), as the 6pAgCl developed into a concave octahedrons, the <100> orthogonal blades on the adjacent pods grew until their edges joint

Fig. 2 SEM micrographs of precipitated 3D AgCl microstructures under: (A) [Ag⁺] = 2.5 - 10 mM, (B) [Cl⁻] = 0.1 - 2 M, and (C) [NH₄OH] = 0 - 0.3 M. The concentrations were varied over those of the standard condition (Figure 2Ac, 2Bc, and 2Cc). (D) a map of 3D AgCl microstructures revealing the influence of reactant concentrations. The structures were divided into 6 groups circumscribed by the dashed lines. The scale bars are 5 μm (main figures) and 1 μm (insets).

together. The jointed edges created triangular vacancies with a tri-pod grove of the growth-suppressed {111} facets. When the NH₄OH concentration was further increased to 0.3 M (Fig. 2Ch), the edges of the concave octahedrons over grown along the <100> directions until the triangular vacancies were filled. The caged octahedron then transformed into an octahedron bounded by {111} facets.

Journal Name

RSC**Publishing**

ARTICLE

Table 1. Experimental condition for the selective fabrication of 3D AgCl microstructures. The concentration and mole ratio are given with respect to those in Fig. 2.

| Fig.	$[Ag^+]$ (M)	$[Cl^-]$ (M)	$[NH_4OH]$ (M)	R1	R2	Products	Group	Note
Effect of $[Ag^+]$								
2Aa	2.5×10^{-3}	1	0.15	400	60	8pAgCl with fishbone triangular pods	VI	++
2Ab	3.5×10^{-3}	1	0.15	285	43	8pAgCl, 6x4pAgCl	III	++
2Ac	**5×10^{-3}**	**1**	**0.15**	**200**	**30**	**8pAgCl, 6x4pAgCl**	**III**	**++**
2Ad	7.5×10^{-3}	1	0.15	133	20	8pAgCl, 6pAgCl, concave cube	II	+++
2Ae	1×10^{-2}	1	0.15	100	15	sphere	I	+++
Effect of $[Cl^-]$								
2Ba	5×10^{-3}	0.1	0.15	20	30	sphere	I	++
2Bb	5×10^{-3}	0.5	0.15	100	30	8pAgCl, 6pAgCl, concave cube	II	++
2Bc	**5×10^{-3}**	**1**	**0.15**	**200**	**30**	**8pAgCl, 6x4pAgCl**	**III**	**++**
2Bd	5×10^{-3}	1.5	0.15	300	30	8pAgCl with fishbone triangular pods	VI	+++
2Be	5×10^{-3}	2	0.15	400	30	8pAgCl with fishbone triangular pods	VI	+++
Effect of $[NH_4OH]$								
2Ca	5×10^{-3}	1	0	200	0	sphere	I	+++
2Cb	5×10^{-3}	1	0.1	200	20	8pAgCl, 6pAgCl, concave cube	II	+++
2Cc	**5×10^{-3}**	**1**	**0.15**	**200**	**30**	**8pAgCl, 6x4pAgCl**	**III**	**++**
2Cd	5×10^{-3}	1	0.2	200	40	6pAgCl, 8x3pAgCl	IV	++
2Ce	5×10^{-3}	1	0.22	200	44	6pAgCl with 4-blade arrowhead pods	V	++
2Cf	5×10^{-3}	1	0.25	200	50	6pAgCl with 4-blade arrowhead pods	V	++
2Cg	5×10^{-3}	1	0.27	200	54	caged octahedron	V	+
2Ch	5×10^{-3}	1	0.3	200	60	octahedron	V	+

Note: +++ precipitate instantaneously
  ++ precipitate within 1 min
  + precipitate within 4 min
  R1 = $[Cl^-]/[Ag^+]$
  R2 = $[NH_4OH]/[Ag^+]$

CrystEngComm Accepted Manuscript

To simplify the structural development under an influence of all three reacting components, 3D AgCl microstructures were projected on a triangular map (Fig. 2D). The microstructures can be classified into six groups. Group I consisted of microspheres that rapidly precipitated at high Ag^+ concentration with relatively low Cl^- and NH_4OH concentration (Table 1). Group II consisted of small concave cubes, 8pAgCl, and 6pAgCl formed at moderate Cl^- and NH_4OH concentrations. As the NH_4OH concentration was increased, group III microstructure consisting of 8pAgCl and 6x4pAgCl was obtained. When NH_4OH concentration further increased, group IV microstructure containing 6pAgCl and 8x3pAgCl was obtained. At extremely high NH_4OH concentration, group V microstructure (6pAgCl, 6pAgCl with 4-blade arrowhead, concave octahedrons and octahedrons) was precipitated. At extremely high Cl^- concentration, the 8pAgCl with triangular pod and 8pAgCl with fishbone triangular pods were obtained (group VI microstructure).

The variation of 3D AgCl microstructures shown in Fig. 2 suggested that Cl^- and NH_4OH played an important role on the structural development. The preferential growth along <111> directions was promoted in Cl^--rich environment.[23, 24] However, the preferential growth along <100> directions in an NH_4OH-rich environment that produced six-pod family has never been reported. To gain an insight understanding on the role of NH_4OH, dissolution of cubic, truncated cubic, and octahedral AgCl by NH_4OH were investigated. The cubes turned into quasi-spheres within a 2-min rinsing by 0.1 M NH_4OH, as shown in Fig. 3A indicating a faster dissolution of {111} corners than {110} edges and {100} facets, respectively. The same phenomena were also observed during the dissolution of truncated cube as the predominant dissolution occurred at the truncated {111} facets (Fig. 3B). The selective dissolution of {111} facets was clearly evident in the octahedrons (Fig. 3C). Surprisingly, after a 2-min rinsing with 0.5 M NH_4OH, the six {100} tips of the octahedrons remained (Fig. 3Cc). The observed structural change in Fig. 3 suggested that NH_4OH preferentially etched the {111} facets. The etching was predominant at the {111} corners and the {110} edges of the cube as well as the {111} facets of octahedrons. The {100} square tips of the octahedron were not disturbed even under a treatment with higher concentration of NH_4OH (Fig. 3C).

When cubic AgCl was incubated in the NH_4OH solution, the transformation of cubes into big truncated cubes indicates the growth in the <100> directions as shown in Fig. 4. The structural change indicates a preferred structural transformation towards that with a greater fraction of {111} facets. An appearance of small microspheres indicates that the formation of bigger truncated cube involved Ostwald ripening. The structural transformations in Fig. 3 and 4 imply a selective preservation of octahedral seeds in the NH_4OH-rich environment where the cubic seeds are selectively destroyed. The structural transformation of fcc crystal (Ag and Pd) from cubes to truncated cubes and octahedrons has been reported.[28, 29]

According to the classified structures in Fig. 2D and Table 1, a structural evolution in the Cl^--rich and NH_4OH-rich growth environment is summarized in Fig. 5. Based on the minimum surface energy hypothesis,[23, 30] we proposed that cubic seeds were firstly developed during the early stage of nucleation as it is the most thermodynamically favorable
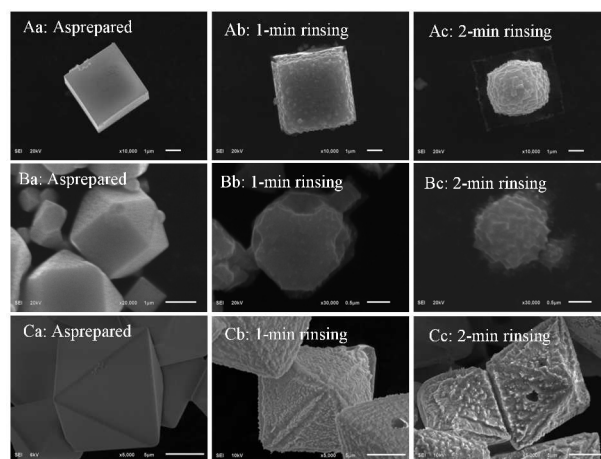

Fig. 3 The dissolution of AgCl by NH_4OH (A) cube, (B) truncated cube, and (C) octahedrons. The etching was performed by continuously rinsing the immobilized AgCl microstructures with 0.1 M NH_4OH (A and B) and 0.5 M NH_4OH (C).

structure. The survival of the seed, the structural transformation, and further development were dictated by the growth environment. With the presence of NH_4OH, the cubic seeds were truncated and transformed into octahedral seeds. Under the moderate condition, both octahedral and cubic seeds survived and further growth into group II structure.

The development of 6x4pAgCl (Group III structure) indicates the conversion of growth from <100> to <111> directions while that of 8x3pAgCl (Group IV structure) indicates the opposite phenomena. The conversion on the preferential growth direction indicates the influence of seed morphology and the growth environment on the final microstructures. The initial growth is dictated by the seed morphology while the concomitant growth is governed by the environment. For 6x4pAgCl, initially, the tips of the octahedral seed grew along the <100> into a small 6pAgCl under a moderate concentration of NH_4OH. Each pod is bound by five {100} facets, eight {110} edges, and four {111} corners (Fig. S3). However, the environment favored the Cl^--induced growth, the small 6pAgCl further grew along <111> directions from the twenty four corners of the six pods into a 6x4pAgCl. Similarly, in the case of 8x3pAgCl, the cubic seed grew along the <111> directions into 8pAgCl with square pods under a moderate Cl^- concentration. However, the tip of each pod was truncated as the seed was grown in an NH_4OH-rich environment (i.e., similar to those in Fig. 4). The crystals then further growth along the <100> directions from the twenty four tips of eight pods into an 8x3pAgCl (Fig. S4).

The previous reports have proven that the octapod AgCl microstructures were grown from cubic seed under the preferential growth along <111> directions in Cl^--rich environment without a presence of NH_4OH.[23, 24] We hypothesize that the six-pod family (Group V microstructure shown in Fig. 2D) was developed from octahedral seeds where NH_4OH plays a major role on the formation and survival of the seeds. A similar phenomenon was reported where the single-crystalline nano-hexapod silver was grown from an octahedral seed.[31] To verify our hypothesis, the time
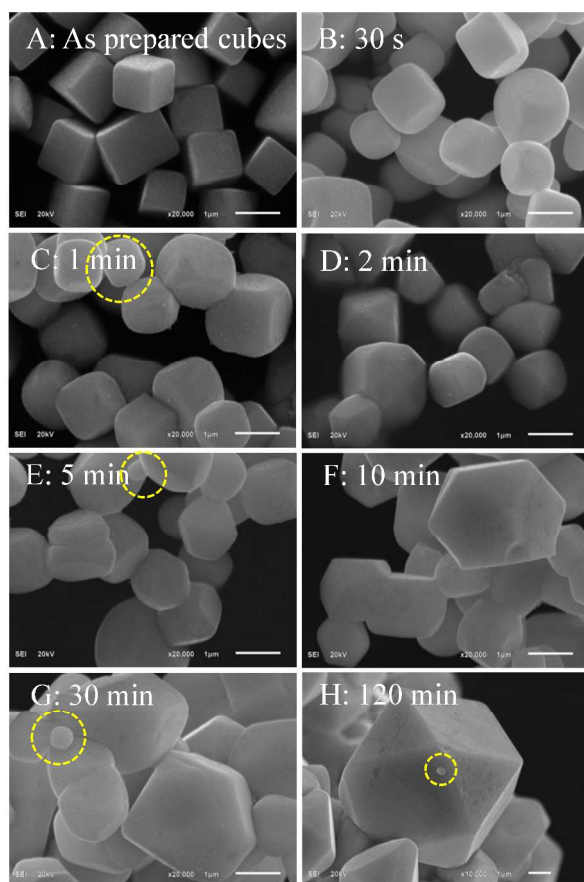
Fig. 4 The structural transformation of cubic AgCl to bigger truncated cubes under the influence of NH₄OH: (A) as prepared cubes, and after an addition of NH₄OH for (B) 30 s, (C) 1 min, (D) 2 min, (E) 5 min, (F) 10 min, (G) 30 min, and (H) 120 min. The scale bars are 1 μm.

_____

dependent structural evolution of several microstructures was investigated and the results are shown in Fig. 6.

The 8pAgCl grew out of cubic seeds while the 6pAgCl and octahedrons grew out of octahedral seeds (Fig. 6, S5, and S6). The nucleation and growth of 3D AgCl microstructures are rapid as they are completed within 5 min. The square pods in 6pAgCl symmetrically grew out in the <100> directions of the tips of octahedral seeds. According to the crystallographic facets, the development of triangular groove corroborates that the six pods of 6pAgCl grew out of the tips of the octahedral seeds not from the face of the cubic seeds. Their square pods developed into 4-blade arrowhead pods. The rapid growth at high NH₄OH concentration connected the orthogonal blades on adjacent pods and the structure was transformed into concave octahedrons and octahedrons, respectively, as shown in Fig. 6E-F.

The XRD patterns of 3D AgCl microstructures in Fig. S7 show characteristic diffraction peaks of (111), (200), (220), (311) and (222) planes indexed to the fcc structure of AgCl (JCPDS No. 85-1355). All diffractions except that of octahedrons showed a more intense (200) peak compared to (111) peak as the structures were dominated by the {100} facets. As the octahedrons are encased by {111} facets, the
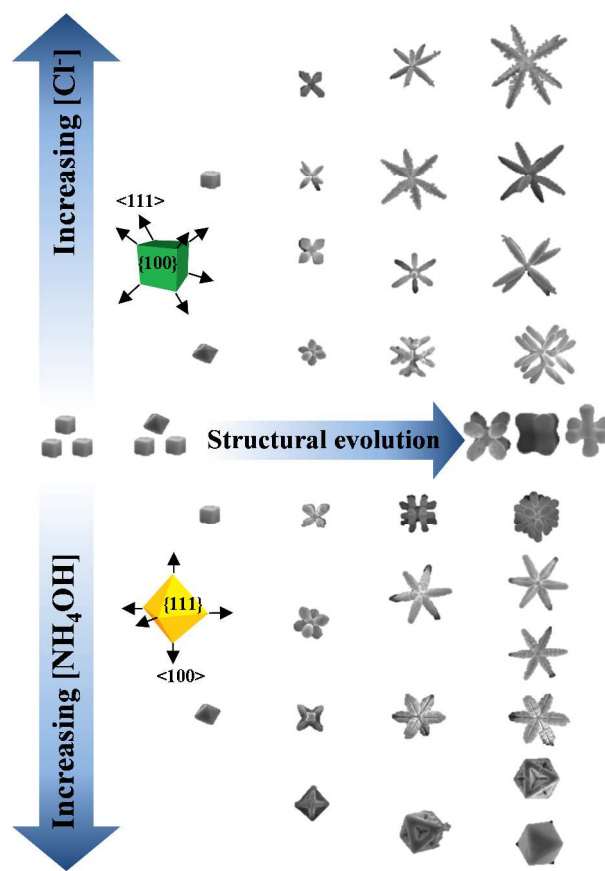

Fig. 5 Schematic illustration shows seed selectivity and concomitant structural development of 3D AgCl microstructures under the influence of Cl⁻ and NH₄OH.

_____

(111) peak is more pronounced with the intensity ratio of peak (111) to that of (200) greater than 1.

To explore their potential application, the morphologically-controlled 3D AgCl microstructures were converted to porous silver microstructure and silver nanoparticle-decorated AgCl microstructures. The porous silver microstructures were prepared by a chemical reduction of 6pAgCl with 4-blade arrowhead using 0.5 M L-ascorbic acid (L-AA). The size and shape of the grey nanoporous silver microstructures are the same as those of original AgCl (Fig. 7A). However, when the AgCl microstructures were briefly treated with a diluted L-AA solution (0.2 M), only surface AgCl was reduced into silver nanoparticle (AgNP) thin film covering the AgCl microstructures (Fig. 7B and S8) which has a dark brown color. When the AgCl microcrystals were reduced via an electron beam bombardment, domains of large AgNPs developed (Fig. 7C and S8). The photocatalytic activities of the synthesized 3D AgCl microstructures were also experimentally compared with that of dendritic silver microstructure synthesized by a previously report technique.[16]

The transformation to nanoporous silver microstructures indicates that the 3D AgCl microstructures can be employed as a building block for the fabrication of complex micro/nanostructures unachievable via a conventional means.[32, 33] The obtained porous silver microstructures could

Journal Name

ARTICLE
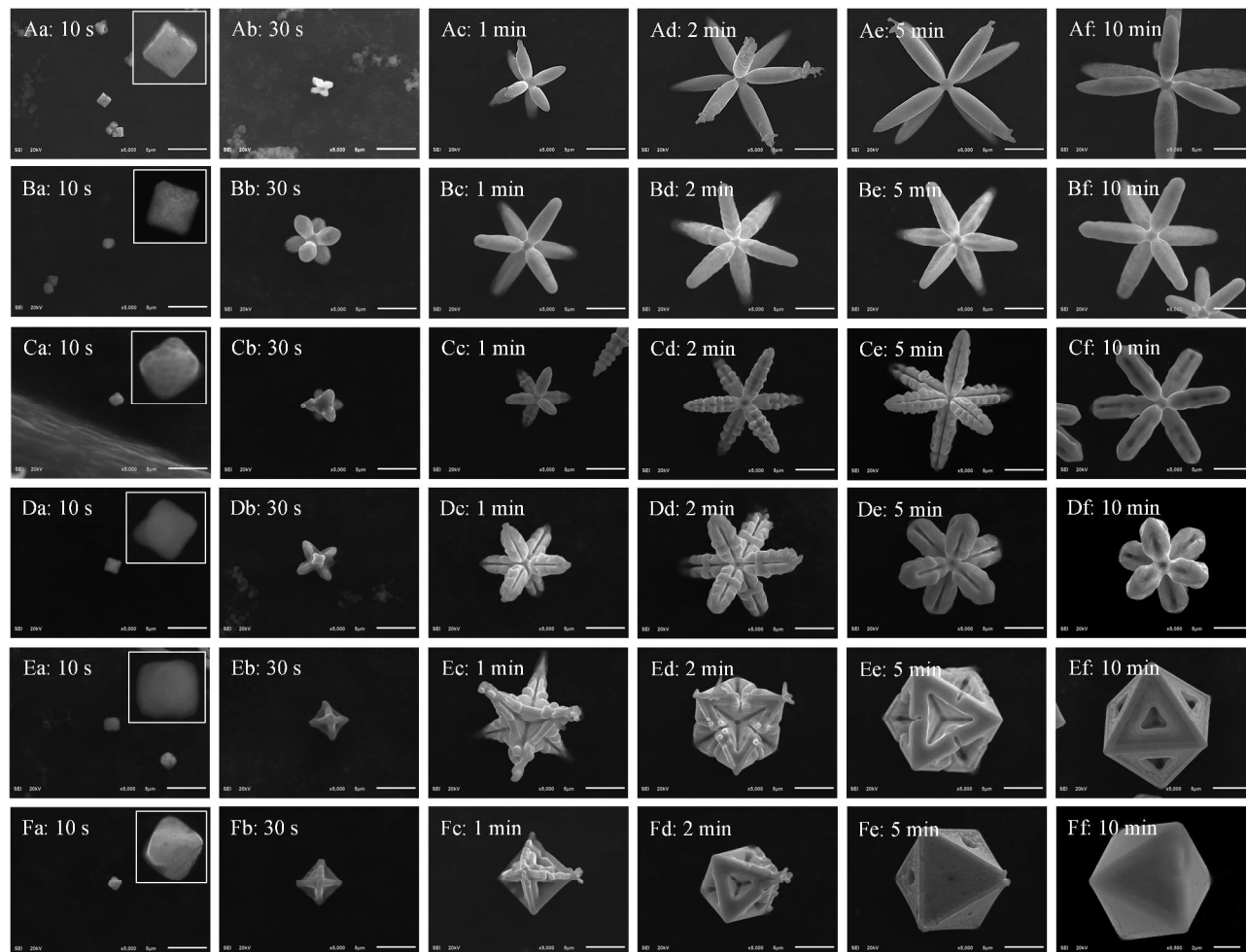
Fig.6 The time dependent structural evolution of (A) 8pAgCl, (B) 6pAgCl, (C and D) 6pAgCl with 4-blade arrowhead, (E) caged octahedron, and (F) octahedron. The structures fully developed within 5 min. The scale bars are 5 µm.

be further employed as a template for surface modifications as well as porous catalysts.[34-38]

The decomposition of methyl orange (MO) under the visible-light-induced photocatalytic activity of 3D AgCl microstructures was investigated. As shown in Fig. 8A, the porous 6pAgCl and AgNP film on AgCl did not exhibit photocatalytic activity. Freshly prepared 3D AgCl microstructures of 8pAgCl with fishbone, 6pAgCl with 4-blade arrowhead, concave octahedrons, and octahedrons expressed moderate photocatalytic activity as 20 - 40% drop of MO concentration was achieved after a 20-min irradiation. The pre-exposed AgCl microstructures were excellent photocatalysts as 8pAgCl and 6pAgCl induced a completed decomposition after a 20-min irradiation as shown in Fig. 8B. The increased catalytic activity was due to the formation of isolated AgNPs as indicated by SEM micrographs and XRD patterns shown in Fig. S8 and S9.[10, 23, 24] The increasing of catalytic activities of Ag@AgCl microstructures was due to the ultrafast plasmon-induced electron transfer processes.[12-14, 16, 18, 19, 22, 39-41] The oscillating dipole on isolated AgNPs enable an oxidation of MO anchored to the surface of AgNPs as surface plasmon resonance (SPR) of AgNPs upon a visible-light irradiation triggers an electron transfer from AgNPs to AgCl. The photocatalytic effect exploits the ultrafast plasmon-induced electron transfer from AgNPs to AgCl. A large numbers of isolated AgNPs become crucial for an efficient photocatalytic activity. As the frequency of the oscillating dipole is unique to the nano-size silver particles, the bulk-like AgNP film and porous silver microstructure do not show a photocatalytic activity since they do not exhibit SPR in the visible region.
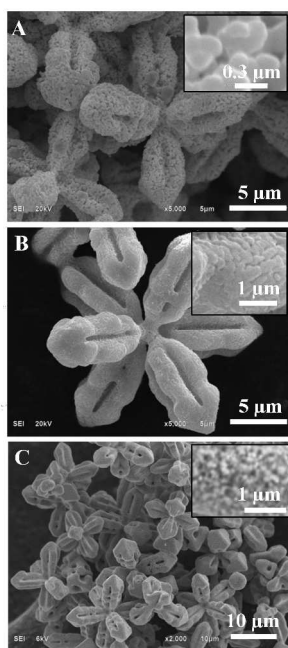
Fig. 7 (A) Nanoporous silver microstructures derived from the 6pAgCl with 4-blade arrowhead pods using 0.5 M L-AA as the reducing agent. AgNP film on AgCl prepared by (B) a partial reduction with 0.2 M L-AA (flash reduction) and (C) an electron beam bombardment in SEM sample chamber.

_____

A repeating usage of the Ag@AgCl photocatalyst was explored and a 40% drop of the catalytic activities was observed after 10 test cycles, as shown in Fig. S10 and S11 (note: the exposure time was kept at 28 min). The decreased catalytic efficiency was due to the formation and increasing of large AgNPs on the surface of Ag@AgCl photocatalyst upon repeated exposures (Fig. S12). The EDX results confirm the increment of silver content as Ag/Cl ratio was increasing from 1.05 (virgin) to 1.12 (1st exposure) and 1.32 (10th exposure), respectively, as shown in Fig. S13 and Table S1. A slightly greater than unity of the ratio in the virgin AgCl microstructures is due to the decomposition of AgCl under the exposure of electron beam.[32] The formation of AgNPs was also confirmed by XRD characterization (Fig. S8) as the characteristic peaks of the fcc silver crystal developed after the 1st exposure.

Surprisingly, the 6pAgCl with 4-blade arrowhead pods was very stable as an insignificant structural change was not observed after the 10th test cycle (Fig. S13). Moreover, a structural break down due to agitation was not observed. However, in the case of 8pAgCl with fishbone pods, the structure broke down after a 10-cycle photocatalytic test. The pods broke down at the joint into rod-like structures as the fishbone feature transformed into AgNPs upon irradiation.

The 6pAgCl with 4-blade arrowhead pods and 8pAgCl with fishbone pods were also excellent photocatalyst for methylene blue (MB) degradation as they can decompose more than 95% of the original concentration within a 28-min irradiation (Fig. S14 and S15).
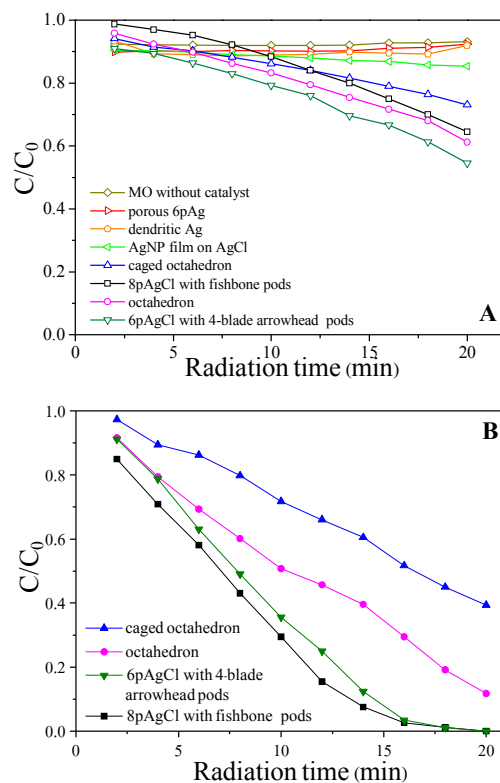
Fig. 8 Catalytic decomposition profiles of MO under the visible light irradiation using (A) freshly prepared 3D AgCl microstructures and (B) Ag@AgCl microstructures as photocatalysts. The photocatalysts included dendritic Ag, nanoporous 6pAg microstructures, AgNP film on 6pAgCl, 8pAgCl with fishbone pods, 6pAgCl with 4-blade arrowhead pods, caged octahedral, and octahedral AgCl

_____

Conclusion

We have successfully developed a simple, rapid, and template-free technique for a selective fabrication of structurally controlled 3D AgCl microstructures via a precipitation from $[Ag(NH_3)_2]^+$ by an addition of Cl- where seed morphology and growth environment dictate the final microstructure. The eight-pod family (8pAgCl and 8pAgCl with fishbone pods) grew from the cubic seeds in Cl--rich environment. The six-pod family (6pAgCl, 6pAgCl with 4-blade arrowhead pods, caged octahedral, and octahedral AgCl), on the other hand, grew from an octahedral seeds NH4OH-rich environment. The 8x3pAgCl microstructures are obtained as the cubic seeds grow in an NH4OH-rich environment while the 6x4pAgCl microstructures are obtained when the octahedral seeds are grown in a Cl--rich environment. The 3D AgCl microstructures can be employed as a building block for the fabrication of novel structures such as nanoporous silver microstructures with controllable pore size. The precipitated 3D AgCl microstructures became an efficient Ag@AgCl visible-light photocatalyst by a partial photo-reduction of the surface AgCl into isolated AgNPs.

Acknowledgements

Development and Promotion of Science and Technology Talents (DPST) Project.

Notes and references

Sensor Research Unit, Department of Chemistry, Faculty of Science, Chulalongkorn University 254 Phyathai Road, Patumwan, Bangkok 10330, Thailand
E-mail: sanong.e@chula.ac.th
Electronic Supplementary Information (ESI) available: [details of any supplementary information available should be included here]. See DOI: 10.1039/b000000x/

1. Y. Xia, Y. Xiong, B. Lim and S. E. Skrabalak, *Angew. Chem. Int. Ed.* 2009, **48**, 60-103.

2. S. Maksimuk, X. Teng and H. Yang, *J. Phys. Chem. C* 2007, **111**, 14312-14319.

3. S. Cheong, J. Watt, B. Ingham, M. F. Toney and R. D. Tilley, *J. Am. Chem. Soc.* 2009, **131**, 14590-14595.

4. M. J. Mulvihill, X. Y. Ling, J. Henzie and P. Yang, *J. Am. Chem. Soc.* 2009, **132**, 268-274.

5. L. Dai, Q. Chi, Y. Zhao, H. Liu, Z. Zhou, J. Li and T. Huang, *Mater. Res. Bull.* 2014, **49**, 413-419.

6. L. Ma, C. Wang, M. Gong, L. Liao, R. Long, J. Wang, D. Wu, W. Zhong, M. J. Kim, Y. Chen, Y. Xie and Y. Xiong, *ACS Nano*, 2012, **6**, 9797-9806.

7. J. Chen, T. Herricks and Y. Xia, *Angew. Chem.* 2005, **117**, 2645-2648.

8. M. Jin, H. Zhang, Z. Xie and Y. Xia, *Angew. Chem. Int. Ed.* 2011, **50**, 7850-7854.

9. T. Yu, D. Y. Kim, H. Zhang and Y. Xia, *Angew. Chem. Int. Ed.* 2011, **50**, 2773-2777.

10. R. Dong, B. Tian, C. Zeng, T. Li, T. Wang and J. Zhang, *The J. Phys. Chem. C* 2012, **117**, 213-220.

11. T. Parnklang, C. Lertvachirapaiboon, P. Pienpinijtham, K. Wongravee, C. Thammacharoen and S. Ekgasit, *RSC Adv.* 2013, **3**, 12886-12894.

12. P. Wang, B. Huang, X. Qin, X. Zhang, Y. Dai, J. Wei and M.-H. Whangbo, *Angew. Chem. Int. Ed.* 2008, **47**, 7931-7933.

13. P. Wang, B. Huang, Q. Zhang, X. Zhang, X. Qin, Y. Dai, J. Zhan, J. Yu, H. Liu and Z. Lou, *Chem. Eur. J.* 2010, **16**, 10042-10047.

14. P. Wang, B. Huang, X. Zhang, X. Qin, H. Jin, Y. Dai, Z. Wang, J. Wei, J. Zhan, S. Wang, J. Wang and M.-H. Whangbo, *Chem. Eur. J.* 2009, **15**, 1821-1824.

15. Q. Zhang, J. Ge, T. Pham, J. Goebl, Y. Hu, Z. Lu and Y. Yin, *Angew. Chem. Int. Ed.* 2009, **48**, 3516-3519.

16. L. Cheng, C. Ma, G. Yang, H. You and J. Fang, *J. Mater. Chem.A* 2014, **2**, 4534-4542.

17. K. i. Kimijima and T. Sugimoto, *J. Phys. Chem. B* 2004, **108**, 3735-3738.

18. M. Zhu, P. Chen and M. Liu, *Langmuir*, 2013, **29**, 9259-9268.

19. C. An, S. Peng and Y. Sun, *Adv. Mater.* 2010, **22**, 2570-2574.

20. D. Chen , S. H. Yoo, Q. Huang, G. Ali and S. O. Cho, *Chem. Eur. J.* 2012, **18**, 5192-5200.

21. Z. Lou, B. Huang, Z. Wang, X. Qin, X. Zhang, Y. Liu, R. Zhang, Y. Dai and M.-H. Whangbo, *Dalton Trans.* 2013, **42**, 15219-15225.

22. Y. Tang, Z. Jiang, G. Xing, A. Li, P. D. Kanhere, Y. Zhang, T. C. Sum, S. Li, X. Chen, Z. Dong and Z. Chen, *Adv. Funct. Mater.* 2013, **23**, 2932-2940.

23. Z. Lou, B. Huang, X. Ma, X. Zhang, X. Qin, Z. Wang, Y. Dai and Y. Liu, *Chem. Eur. J.* 2012, **18**, 16090-16096.

24. Z. Lou, B. Huang, X. Qin, X. Zhang, H. Cheng, Y. Liu, S. Wang, J. Wang and Y. Dai, *Chem. Commun.* 2012, **48**, 3488-3490.

25. I. Maudos, J. M. Chimenos, M. Segarra and F. Espiell, *Hydrometallurgy*, 1996, **40**, 153-167.

26. R. L. David, ed., *CRC Handbook of Chemistry and Physics*, 90th Edition (CD-ROM Version 2010) edn., CRC Press, Boca Raton, Florida, 2010.

27. R. Nasanen, *Acta Chem. Scand.* 1947, **1**, 763-769.

28. X. Xia, J. Zeng, Q. Zhang, C. H. Moran and Y. Xia, *The J. Phys. Chem. C.* 2012, **116**, 21647-21656.

29. H. Zhang, M. Jin, Y. Xiong, B. Lim and Y. Xia, *Acc. Chem. Res.* 2012, **46**, 1783-1794.

30. X. Ma, Y. Dai, J. Lu, M. Guo and B. Huang, *J. Phys. Chem. C.* 2012, **116**, 19372-19378.

31. X. Liu, F. Zhang, R. Huang, C. Pan and J. Zhu, *Cryst. Growth Des.* 2008, **8**, 1916-1923.

32. E. V. Formo, W. Fu, A. J. Rondinone and S. Dai, *RSC Adv.* 2012, **2**, 9359-9361.

33. X. Luo, S. Lian, L. Wang, S. Yang, Z. Yang, B. Ding and X. Song, *CrystEngComm*, 2013, **15**, 2588-2591.

34. J. Chen, B. Wiley, J. McLellan, Y. Xiong, Z.-Y. Li and Y. Xia, *Nano Lett.* 2005, **5**, 2058-2062.

35. X. Lu, H.-Y. Tuan, J. Chen, Z.-Y. Li, B. A. Korgel and Y. Xia, *J. Am. Chem. Soc.* 2007, **129**, 1733-1742.

36. X. Hong, D. Wang, S. Cai, H. Rong and Y. Li, *J. Am. Chem. Soc.* 2012, **134**, 18165-18168.

37. Q. Zhang, Y. H. Lee, I. Y. Phang, S. Pedireddy, W. W. Tjiu and X. Y. Ling, *Langmuir*, 2013, **29**, 12844-12851.

38. J. Li, W. Yang, J. Ning, Y. Zhong and Y. Hu, *Nanoscale*, 2014, DOI: 10.1039/c4nr00364k.

39. D. Chen, M. Liu, Q. Chen, L. Ge, B. Fan, H. Wang, H. Lu, D. Yang, R. Zhang, Q. Yan, G. Shao, J. Sun and L. Gao, *Appl. Catal., B* 2014, **144**, 394-407.

40. L. Ai, C. Zhang and J. Jiang, *Appl. Catal., B.* 2013, **142–143**, 744-751.

41. J. Jiang and L. Zhang, *Chem. Eur. J.* 2011, **17**, 3710-3717.

CrystEngComm Accepted Manuscript